PASJ: Publ. Astron. Soc. Japan **61**, 1–12, 2009 February 25

The Atacama Compact Array (ACA)

Satoru IGUCHI,[1] Koh-Ichiro MORITA,[1] Masahiro SUGIMOTO,[1] Baltasar VILA VILARÓ,[1] Masao SAITO,[1] Tetsuo HASEGAWA,[2] Ryohei KAWABE,[3] Ken'ichi TATEMATSU,[1] Seiichi SAKAMOTO,[4] Hitoshi KIUCHI,[1] Sachiko K. OKUMURA,[1] George KOSUGI,[1] Junji INATANI,[1] Shigehisa TAKAKUWA,[5] Daisuke IONO,[3] Takeshi KAMAZAKI,[1,6] Ryusuke OGASAWARA,[7] and Masato ISHIGURO[8]

[1]*National Astronomical Observatory of Japan (NAOJ), 2-21-1 Osawa, Mitaka, Tokyo 181-8588*
[2]*Joint ALMA Office, El Golf 40, Piso 18, Las Condes, Santiago 755-0108, Chile*
[3]*Nobeyama Radio Observatory, 462-2 Nobeyama, Minamimaki, Minamisaku, Nagano 384-1305*
[4]*Institute of Space and Astronautical Science, 3-1-1 Yoshinodai, Sagamihara, Kanagawa 229-8510*
[5]*Academia Sinica Institute of Astronomy and Astrophysics, PO Box 23-141, Taipei 10617, Taiwan, R.O.C.*
[6]*NAOJ ALMA Chile Office, Operations Support Facility Branch Office, KM 121 CH 23, San Pedro de Atacama, II Región, Chile*
[7]*NAOJ ALMA Chile Office, Santiago Head Office, El Golf 40, Piso 18, Las Condes, Santiago 755-0108, Chile*
[8]*Joint ALMA Office, Avda. Apoquindo 3846, Piso 19, Edificio Alsacia, Las Condes, Santiago 755-0108, Chile*
s.iguchi@nao.ac.jp

(Received 2008 April 15; accepted 2008 September 2)

Abstract

For realizing high fidelity of imaging with mosaicing observations, the Atacama Large Millimeter/submillimeter Array (ALMA) consists of a homogeneous array of 12 m antennas (12 m Array) and the Atacama Compact Array (ACA) in order to cover all spatial frequency Fourier components of the brightness distribution of observed sources. The array is located at an altitude site of about 5000 m with an operating wavelength range of 0.3 to 3 mm. ACA is an array composed of four 12 m dishes [TP (Total Power) Array] and twelve 7 m dishes (7 m Array). The 7 m Array has a very compact configuration to take short-baseline data corresponding to the low spatial frequency Fourier components. The 7 m Array has two configurations extended over 30–50 m to avoid shadowing at low elevation. The scientific importances and operation concepts of ACA, and the system design of ACA and its performance are presented in this paper.

Key words: instrumentation: interferometers — radio continuum: general — radio lines: general — techniques: image processing — techniques: interferometric

1. Introduction

Several large millimeter/submillimeter array projects were conceptualized in the 1980s [i.e., Millimeter Array (MMA), Large Millimeter Array (LMA)/ Large Millimeter Submillimeter Array (LMSA), and Large Southern Array (LSA)] as next-generation instruments in quest of higher sensitivity and spatial resolution (Vanden Bout 2005). With the aim of realizing an ultimate synthesis telescope at millimeter/submillimeter wavelengths, the Atacama Large Millimeter/submillimeter Array (ALMA) is being built by collaboration among Europe, Japan, and North America. It is located on the Chajnantor Altiplano in the Atacama Desert of Northern Chile at an altitude of about 5000 m, and operated by a trilateral partnership (Beasley et al. 2006). ALMA will allow us to make specific quantitative studies of high importance: cool atomic gas, molecular gas and dust in the universe, which form stars, planets, and galaxies, and moreover kinetic energy, and the gas mass and density distribution law in protoplanetary disks and molecular envelops around newly born stars. Finally, ALMA is expected to have impacts on at least three important scientific fields: the formation and history of galaxies, the formation of extraterrestrial planetary systems, including the emergence of the life, and the history of the universe from the Big Bang.

The emissions from cool atomic gas, molecular gas, and dust are mostly thermal, and their structures are extended. For their quantitative studies, spatially resolved observations are desirable using ALMA. To image extended emission structures at high angular resolution, ALMA needs to cover all spatial frequency Fourier components of their brightness distribution. ALMA consists of a homogeneous array of 12 m diameter antennas for the interferometer (12 m Array) and the Atacama Compact Array (ACA). ACA is a short-spacing imaging system consisting of four 12 m antennas for Total Power observations (TP Array) and twelve 7 m antennas for interferometry (7 m Array). The conceptual design of ACA is described in section 2, the scientific operations in section 3, and the system in section 4; the performance and expected science enhancement of ACA are discussed in section 5.

2. The Conceptual Design of ACA

2.1. The Concept and Purpose of ACA

The high imaging fidelity of the extended astronomical sources (the large-scale structure) with an interferometer is one of the issues that demand immediate attention. This is particularly important for a significant part of sources that have most of their emitted power in short spacings. The main problem arises from conflicting constraints of increasing antenna sizes

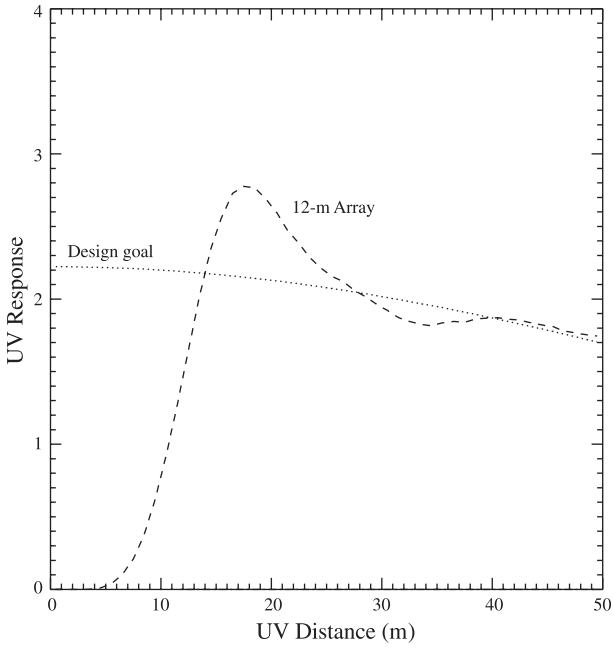

Fig. 1. The *uv* response profiles of a best-fit Gaussian as a design goal (dotted line) and the most compact configuration of the 12 m Array (dashed line), which is similar to a natural *uv* sampling weight, for the case of mosaicing observations at a declination of −23° and a close–packing ratio of 1.25. The *uv* response of the mosaic observation is derived by convolution of a *uv* track with autocorrelation of the voltage illumination of the antenna.

and observations at short spacings. The former increases the collective area of the telescope, and thus the sensitivity, but makes it physically impossible to pack antennas closer than 1.2–1.3 times its diameter. This results in the well-known "missing flux" problem of interferometers, i.e., spatial information at equivalent baselines shorter than the close-packing ratio cannot be recovered (strictly speaking, mosaicing allows the recovery of more spatial information than normal synthesis imaging, but the underlying problem of a lack of short spacing information remains). An increase of the antenna size results in a smaller primary beam size, which leads to a larger missing flux and relative pointing error.

Although the 12 m Array will be a very powerful high-resolution imaging machine, it will require additional information if the short-spacing data are important for a given observational project. Since one of the goals of ALMA is high imaging fidelity, recovering the large-scale structures contained in the short spacings is important and, in fact, crucial for the quantitative studies mentioned above. Solving this problem is essential if ALMA is to provide reliable images to both experts and nonexperts (novice users), because it is sometimes difficult to interpret images without short spacing data.

One of the generic techniques proposed to solve this problem of homogeneous arrays is the inclusion of TP data (taken with the same or larger antennas) and mosaicing (multipointing) interferometric observations (e.g., Cornwell 1988). It was considered in ALMA that total-power data are added by taking with some 12 m antennas in a single-dish mode. However, intermediate baselines of 6–15 m cannot be covered in that case. Short-spacing data can also be measured by using a single-dish telescope with a diameter of at least larger than 20 m. However, to obtain a high-quality image by such a 20 m antenna, the pointing accuracy should be smaller than 1/10 of the beam width, which corresponds to about 0.″4 at 950 GHz. In addition, the requirement is equal or less than the 1st quartile pointing error due to anomalous refraction at Chajnantor (M. Holdaway & J. Woody 1998).[1] A larger single-dish telescope with this requirement is quite expensive compared with a 12 m antenna. These problems can be solved as proposed concerning ACA. Thus, the major goal of introducing ACA is to enable ALMA to image extended objects with high precision and robustness by directly sampling the low spatial frequency visibilities at a *uv* gap of the 12 m Array configuration. See J. Welch (2001)[2] for an approach to the choices of the diameter and number, J. Baars (2000)[3] for the choice of diameter, and Morita and Holdaway (2005) for more quantitative justifications concerning the numbers and diameters.

The adopted solution for ALMA is to add the total-power data obtained from the single-dish observing system and the short-spacing data from an array with smaller dishes that covers the intermediate baselines of 6 to 15 m. Antennas with a 12 m diameter were selected for the TP Array by taking the compatibility into consideration, because the total-power data are also measured with the 12 m Array. The number of antennas for the TP Array was determined to obtain sufficient calibration sensitivity for the ACA system. The 7 m Array was designed according to the sample visibilities at baseline lengths of 6 to 15 m, where the TP Array and the 12 m Array have almost no response. The diameter and the number of element antennas of the 7 m Array were chosen by a discussion of the *uv* response at these short-baseline lengths (Morita & Holdaway 2008). At submillimeter wavelengths, the importance of ACA increases, because the field of view (primary beam) for the 12 m Array decreases inversely in proportion to the observing frequency, and the observing targets become larger than the primary beam width.

In summary, the main scientific requirements for ACA are defined to provide short-baseline data and total-power data with high precision in order to complement the 12 m Array data and to enhance the image fidelity, particularly for extended astronomical sources. It is also expected that ACA will sometimes observe in the stand-alone mode, and thus will have to provide reasonable imaging capabilities for such a situation.

2.2. *The Configurations of ACA*

In imaging, a desirable beam-pattern response (point-spread function) of a telescope should have a single smooth peak without any sidelobes, which cause image estimation errors. Deconvolution methods, like CLEAN or MEM, can compensate such imaging errors, but the thermal noise and the calibration errors by the deconvolution methods often cause serious imaging errors, because most of the deconvolution

[1] ALMA memo No. 223 ⟨http://www.alma.nrao.edu/memos/html-memos/abstracts/abs223.html⟩.
[2] ALMA memo No. 354 ⟨http://www.alma.nrao.edu/memos/html-memos/abstracts/abs354.html⟩.
[3] ALMA memo No. 339 ⟨http://www.alma.nrao.edu/memos/html-memos/abstracts/abs339.html⟩.

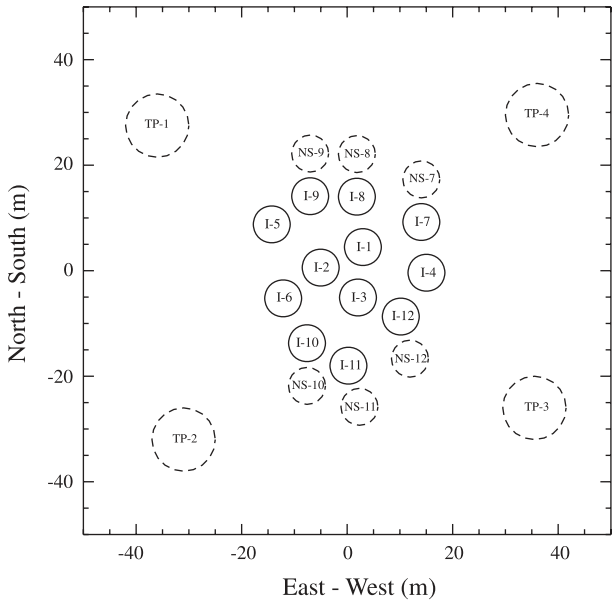

Fig. 2. Configuration of ACA: the Inner Array (solid line), the NS Array (dashed line), and TP Array (dashed line). Antenna pad positions are listed in table 1. The circles are proportional to the sizes of the antennas.

processes are nonlinear.

In the spatial frequency domain (uv domain), the beam-pattern response, such as a Gaussian function, corresponds to a function with a smooth sampling taper. In designing the inner configurations of the 12 m Array, J. Conway (2000)[4] proposed a Gaussian-shape function as a target uv response. This concept was adopted in the ALMA project as the final design. Figure 1 shows an example of the uv response for the case of mosaic observations for a declination of $-23°$ with the most compact configuration of the 12 m Array. Although this profile is very close to the target uv response, the response dips below the "design goal response" fit curve for the distance that is shorter than about 13.5 m (less than 1.25×12 m), and there is no response at all below about 5 m. The image quality is affected by both the sensitivity and the uv sampling (i.e., synthesized beam quality) for the desired baseline spacings. To fill missing areas in the uv gap of the 12 m Array, the configuration of ACA 7 m antennas will be very compact (K. Morita & M. Holdaway 2005).[5]

Due to the smaller point-source sensitivity of the 7 m Array, it is expected that the TP Array will be routinely used in calibration observations (pointing, phase, etc.) of the 7 m Array (by performing the correlations between the TP Array and the 7 m Array). A correction of the fast tropospheric phase fluctuations using the Water Vapor Radiometer (WVR) on each of the TP Array antennas requires that the TP Array be located closely around the 7 m Array (Y. Asaki 2005).[6] In addition, the ACA location will be as close to the compact configuration of the 12 m Array as possible for purposes of accurate cross-calibration.

Table 1. Pad number and location relative to the array center of ACA.*

Pad	East position [m]	North position [m]
TP-1	−36.00	27.50
TP-2	−31.00	−32.00
TP-3	35.50	−26.00
TP-4	36.00	29.50
I-1	2.98	4.48
I-2	−5.02	0.59
I-3	2.05	−5.08
I-4	15.03	−0.38
I-5	−14.29	8.78
I-6	−12.13	−5.24
I-7	14.06	9.23
I-8	1.84	14.03
I-9	−7.01	14.12
I-10	−7.61	−13.74
I-11	0.24	−18.00
I-12	10.17	−8.69
NS-7	14.06	17.30
NS-8	1.84	22.10
NS-9	−7.01	22.20
NS-10	−7.61	−21.83
NS-11	2.33	−25.80
NS-12	11.90	−16.67

* TP-X means the TP Array, I-X means the inner array of the 7 m Array, and NS-X means the NS-array, but central 6 pads are not moved.

The very compact configuration of ACA makes it difficult to access antennas in the center with an antenna transporter and a service vehicle. Regarding the antenna transporter, an access area of 12 m × 30 m should be reserved around the antennas according to the mechanical structure of the antenna transporter. For maintaining the front-end assemblies, the front-end service vehicle should access any of the antennas when it is in normal operation without any antenna movement. A rectangular access area of 4–5 m × 20 m is needed for this purpose.

We adopted a compact spiral design which is similar to the configuration proposed by J. Conway (2000).[7] This design concept was slightly modified to obtain enough uv samples at the minimum spacing. To use 3 logarithmic spirals [$r = \exp(A\theta_{\rm AZ})$], starting from each antenna of the central triangle with the minimum spacing (close packing ratio × antenna diameter), 3 antennas are located on each spiral with an interval of the minimum spacing.

Since the very compact configuration causes significant shadowing in the case of observations at low elevations, relocations of the 7 m antennas will be required in the outer pads to cover both extremes in the declination range. To cover the same declination range as the 12 m Array (of about [−85,40]), the 7 m Array should have two configurations: one (Inner Array) is a compact spiral array with small north–south (NS) elongation, and the other (NS Array) is a dedicated configuration with large NS elongation.

[4] ALMA memo No. 283 ⟨http://www.alma.nrao.edu/memos/html-memos/abstracts/abs283.html⟩.

[5] ALMA memo No. 538 ⟨http://www.alma.nrao.edu/memos/html-memos/abstracts/abs538.html⟩.

[6] ALMA memo No. 535 ⟨http://www.alma.nrao.edu/memos/html-memos/abstracts/abs535.html⟩.

[7] ALMA memo No. 283 ⟨http://www.alma.nrao.edu/memos/html-memos/abstracts/abs283.html⟩.

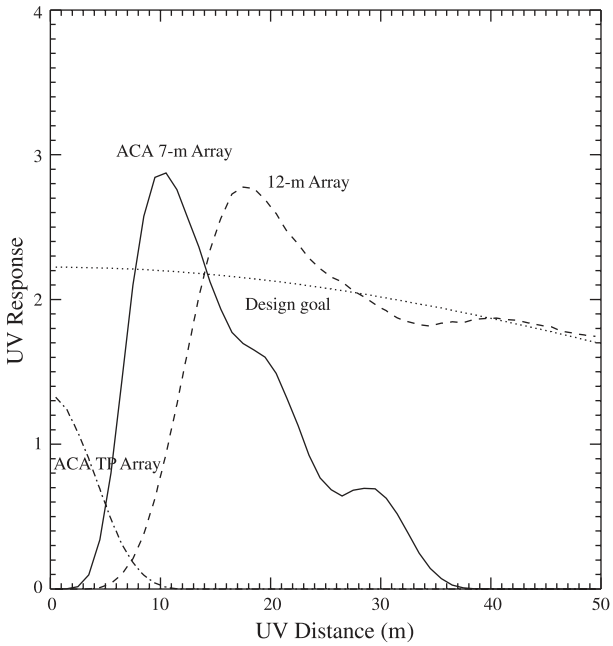

Fig. 3. The *uv* response profiles of a best fit Gaussian as a design goal (dotted line) and the most compact configuration of the 12 m Array (dashed line), the 7 m Array (solid line) and TP Array (dash-dotted line). ACA was added into figure 1.

For the actual design, it is difficult to realize two different pad distributions in the crowded central area of the array. Thus, the central 6 pads are common to the Inner Array and NS Array. The pad positions of ACA are listed in table 1, and the configuration is shown in figure 2. The Inner Array is a compact spiral array with small NS elongation ($\times 1.1$), and the NS Array is a dedicated configuration with large NS elongation ($\times 1.7$). The *uv* responses of the 12 m Array and ACA are shown in figure 3.

3. The Scientific Operations of ACA

We expect that ACA will be easily used by all users. End-to-end scientific services for ACA users will be developed to support this, and will be integrated with those for the 12 m Array. In particular, information on the status and capabilities of ACA, tools that help users to prepare proposals and observations (including ways to ascertain the needs of ACA observations for any given proposal), and a data-quality assurance plan should be developed.

Three types of observations (as the following subsections) are available with ALMA, which consists of the 12 m Array and ACA.

3.1. The Coordinated Operation

Observations of common observing programs using both the 12 m Array and ACA are executed separately. No cross-correlations between the 12 m Array and ACA are obtained. In coordinated observations, the 7 m Array is operated as an interferometer (of single-field mode or mosaicing mode) to take short-baseline data, and the TP Array is operated as four single-dish telescopes (of raster-scan mode or multipointing mode) to take total-power data. The final images with ALMA are obtained by using the usual imaging algorithm, in which the visibility data at the baselines of 0–6 m are derived from a Fourier transform of the total-power data, and then combined with the visibility data from the 7 m Array and the 12 m Array in the *uv* plane. This is a major-observing mode for ACA.

The ACA full Array (7 m Array and TP Array) is simultaneously operated as one interferometer for calibrating the overall system of ACA; e.g., baseline, pointing, phase and amplitude calibrations, bandpass, etc.

3.2. The Combined Operation

The combined array (or heterogeneous array), composed of the 12 m Array and ACA, will be operated as an interferometer. The combined-array mode of observation significantly increases the point-source sensitivity of ACA, and can thus be used to achieve high-quality ACA calibration accuracy for projects that require it (in particular for cross-calibration, bandpass, polarization, etc.).

3.3. ACA Stand-Alone Operation

Although not a major scientific operation mode, ACA will provide a stand-alone operation mode. The available observing modes will be identical for coordinated observations. Particularly, when the 12 m Array has the extended configuration, excellent targets for such a mode are targets of opportunity (ToO) sources; especially extended ToO sources, such as comets and unexpected events in planets, can be handled by ACA at any time, because of the limited changes in the configurations. Projects for extended, bright sources that do not require 12 m Array observations can also be accommodated; e.g., wide-field imaging of nearby molecular clouds, etc.

4. The System Description and Performance of ACA

ACA will be as compatible with the 12 m Array as possible according to the operation concepts described in section 3. This is therefore a requirement at the level of both the hardware/interface/data and the observing modes that are provided. To achieve this, the following will be the same as for the 12 m Array: a) frequency coverage of all available millimeter and submillimeter atmospheric windows, b) concerning spectral frequency resolutions, the spectral channel numbers should be at least equal for each set-up, c) interband/intraband tuning capabilities and required timescales, d) IF (Intermediate Frequency) bandwidth and processing chains, e) sideband separation schemes and receiving system, f) dual polarization and polarimetry requirements, g) solar observation capabilities, h) elevation range coverage, and i) common TP and interferometric observing modes (except those that require specific hardwares to be installed only at ACA).

4.1. The Frequency Coverage and Receiving System

In the ALMA receiving system, there are three types of receiving systems: a single-sideband (SSB) receiving system, a double-sideband (DSB) receiving system, and a two-single-sideband (2SB) receiving system. Based on the practical environments at the ALMA site, the 2SB receiving system is best at submillimeter and millimeter wavelengths from

Table 2. ALMA receiver bands.

Band	Frequency range (GHz)	Type
1	31.3– 45	SSB
2	67 – 90	SSB
3	84 –116	2SB
4	125 –163	2SB
5	163 –211	2SB
6	211 –275	2SB
7	275 –373	2SB
8	385 –500	2SB
9	602 –720	DSB
10	787 –950	DSB

Table 3. Parameters for the Cassegrain ALMA antennas.

Parameters	12 m ant.*	7 m ant.†
Close packing ratio	1.25	1.25
Primary diameter, D	12 m	7 m
Primary focal length, F	4.800 m	2.5717 m
Secondary diameter, d_s	0.750 m	0.4569 m
Primary focal ratio, F/D	0.4	0.37
Half-angle of primary, θ_p	64°.01	68°.47
Half-angle of secondary, θ_s	3°.58	3°.58
Interfocal distance, $2c$	6.1770 m	3.7417 m
Vertex hole diameter, h	0.750 m	0.750 m

* J. Lamb et al. (1999).[8]
† This paper.

the viewpoint of several astronomical observations, calibration methods, and the astronomical data quality. In Bands 9 and 10, we adopted the DSB receiving system, taking the technical feasibility into consideration (see table 2). The detectable sensitivity of the DSB receiving system in observing a continuum radiation source is improved by the IF range of 4 to 12 GHz, approaching the performance of the 2SB receiving system with the IF range of 4 to 8 GHz (Iguchi 2005).

4.2. The Compatibility of Interface and Data

ACA must be controlled under a common ALMA software system and integrated into a unified operation scheme of the ALMA observatory. To ease this, the specifications and interfaces of the 12 m Array were adopted as much as possible.

Data from ACA should be processed by a common pipeline software system, and they should be combinable off-line with those from the 12 m Array with no degradation of quality of all data sets.

The full 8 GHz IF bandwidth per polarization per antenna must be processed by the entire signal chain, from the front-end element (mixer) through to the correlator. ACA, except for the ACA Correlator, is required to be connected to the 12 m Array electrically for taking cross-correlation data for calibration purposes and actual imaging observations.

The ACA Correlator will realize all observation modes that are realized by using Tunable Filter Bank implemented to the 12 m Array Correlator (Escoffier et al. 2007), and provide the cross-correlations for 120 baselines (a pair of two antennas) and the autocorrelations for 16 antennas. First quantization is 3 bits (8 levels) at a digitizer, and the second requantization will not be less than 4 bits (16 levels) and will be at less than or equal to one place in the ACA Correlator. The highest frequency channel will be less than 6 kHz, or 0.02 km s^{-1} at 100 GHz (referring to Beasley et al. 2006).

4.3. The Optical Design of ACA Antennas

The optical parameter for the 12 m Cassegrain antenna was proposed on the basis of focal plane aberrations, the focal spot size, the blockage, and the feasibility of implementing a nutating subreflector (J. Lamb et al. 1999),[8] and was then adopted in ALMA (Beasley et al. 2006). The requirements of the ACA 12 m antennas are exactly the same as those of the 12 m Array. Four ACA 12 m antennas are equipped with a nutating subreflector.

The Front End (FE) subsystem implemented in the 7 m antennas is the same as that of the 12 m Array and the ACA 12 m antennas (TP Array), even if a redesign for the 7 m receiver optics is required. This selection is due to the viewpoints of reliability, operability, and maintainability, and the avoidance of the duplicate development. If the 7 m antenna optics has the same half-angle of the secondary, θ_s, as that of the 12 m antenna, under the condition that the subreflector is placed far-field from the receiver, the same illumination profiles as those of 12 m antenna can be achieved in 7 m receiver optics. This is a big advantage that the optical components of the 12 m receiver can be used for the 7 m antenna, except for changing the boresight tilt angle of the receiver. The Rayleigh distance of Band 1 receiver, $R = \pi \cdot w_0^2/\lambda$, is about 1000 mm, where w_0 is the beam waist size, 57 mm, and λ is the wavelength, 10 mm (J. Lamb et al. 2001).[9]

This corresponds to about $1/3$ of the distance between the antenna Cassegrain focus and the 7 m subreflector (see $2c$ in table 3). Thus, the condition of far-field is valid for all frequency bands. Figure 4 shows the beam waist positions of the receivers and the defocus loss of 1% loss, giving us a defocus loss of less than 1% when the primary F/D is 0.3. The defocusing effect is most sensitive to the primary F/D ratio, and suggests that the primary F/D ratio should be larger than 0.3. The definition of optics parameters is shown in figure 5. By considering the mechanical structure of the antenna (e.g., weight balance along with the elevation axis), the 7 m antenna optics parameter was defined as tabulated in table 3. The vertex hole diameter of the 7 m antenna is equivalent to that of the 12 m antennas (i.e., 0.75 m) to avoid beam truncations.

4.3.1. Geometrical blocking of ACA antennas

The geometrical blockage is

$$g_b = \frac{\int\int_a dS - \int\int_b dS}{\int\int_a dS}, \quad (1)$$

[8] ALMA memo No. 246 ⟨http://www.alma.nrao.edu/memos/html-memos/abstracts/abs246.html⟩.

[9] ALMA memo No. 362 ⟨http://www.alma.nrao.edu/memos/html-memos/abstracts/abs362.html⟩.

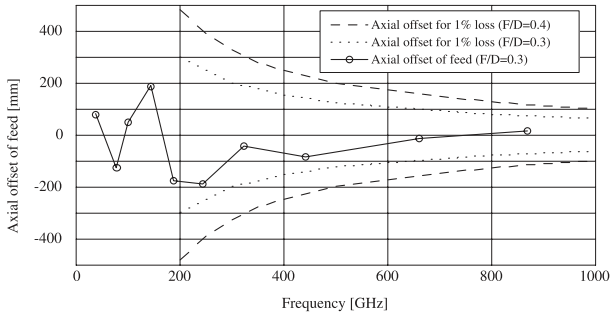

Fig. 4. Axial offset versus frequency of the feed including the Petzval surface effects (solid line), and for the (F/D)s of 0.4 (dashed line) and of 0.3 (dotted line) at a defocus loss of just 1%.

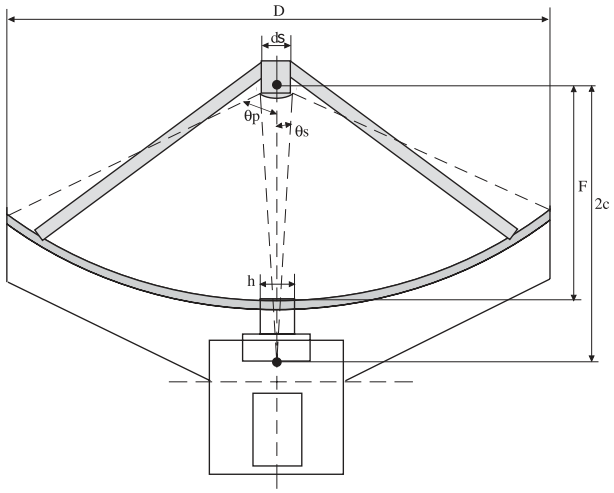

Fig. 5. Optics configuration of the antenna.

where subscript "a" denotes an integral extending over only the area in the antenna aperture, and subscript "b" denotes the area in the aperture plane blocked by the subreflector and four quadripods.

Because the FE subsystem is optimized to design the 12 m antenna, the blockage efficiency of the ACA 7 m antenna will include the effect that the vertex hole diameter of h (= 0.75 m) is larger than the subreflector diameter of d_s (∼ 0.457 m), as shown in figure 6 (see table 3). When w (width of quadripod) is 0.16 m and L (length from the vertex hole) is $(5/6)\cdot(d/2)$ m, the geometrical blockages of 12 m and 7 m antennas become 0.97 and 0.95, respectively.

4.4. *Surface Accuracy and Aperture Efficiency of ACA Antennas*

The ACA 12 m antenna will have surfaces (main- and subreflectors) with illumination-weighted rms deviations from the ideal of 25 μm rms or less (Beasley et al. 2006). Considering that this is the submillimeter observation and that the collecting area of 7 m dish is less than that of 12 m dish, the ACA 7 m antenna will have surfaces (main- and subreflectors) with illumination-weighted rms deviations from the ideal of 20 μm rms.

The total aperture efficiency, η_a, can be estimated from the following factors not related to the details of the feed: the radiation efficiency (ohmic loss), η_o, illumination efficiency, η_i, spillover efficiency, η_s, diffraction efficiency, η_d, Ruze efficiency, η_r, and blockage efficiency, η_b, of the main- and subantenna reflectors.

In general, the optics design of the antenna and the receiver is performed by a best-fit Gaussian beam with an edge taper of 12 dB at the subreflector. This design will give the highest efficiency when the beam is launched by a corrugated feed horn. The aperture field from this ideal corrugated feed horn is approximated closely by the Bessel function of zeroth order, J_0 (see Goldsmith 1998). In this paper, the illumination efficiency, spillover efficiency, and blockage efficiency are estimated while supposing that this assumption is valid for all frequencies.

4.4.1. *Radiation efficiency*

The reflection loss of the metal surface at a frequency of ν [Hz] is described as (see Goldsmith 1998)

$$4\sqrt{\frac{\pi\varepsilon_0\nu}{\sigma}}, \tag{2}$$

and by taking main- and subreflectors into consideration, the radiation efficiency (ohmic loss) is derived as

$$\eta_o = \left(1 - 4\sqrt{\frac{\pi\varepsilon_0\nu}{\sigma}}\right)^2, \tag{3}$$

where ε_0 and σ denote the dielectric constant of free space and the conductivity of material.

4.4.2. *Illumination efficiency and spillover efficiency*

The illumination efficiency and the spillover efficiency are given by

$$\eta_i = \frac{|\int\int_a E_a dS|^2}{\int\int_a |E_a|^2 dS \int\int_a dS} \tag{4}$$

and

$$\eta_s = \frac{\int\int_a |E_a|^2 dS}{\int\int_{ap} |E_a|^2 dS}, \tag{5}$$

where E_a is the field intensity in the aperture plane, and the subscript "ap" denotes an integral extending over the entire aperture plane (see Goldsmith 1998).

4.4.3. *Diffraction efficiency*

Diffraction by the subreflector can be simplified to

$$\eta_d = 1 - 2C_d A_0 \sqrt{\frac{\lambda}{d_s}}, \tag{6}$$

where

$$C_d = \frac{-\ln A_0}{\pi(1 - A_0)}. \tag{7}$$

A_0 is the amplitude ratio of the edge to the center, λ is the wavelength [mm], and d_s is the actual hyperboloid diameter of the subreflector (see figure 6), in the case of Gaussian illumination (see Kildal 1983).

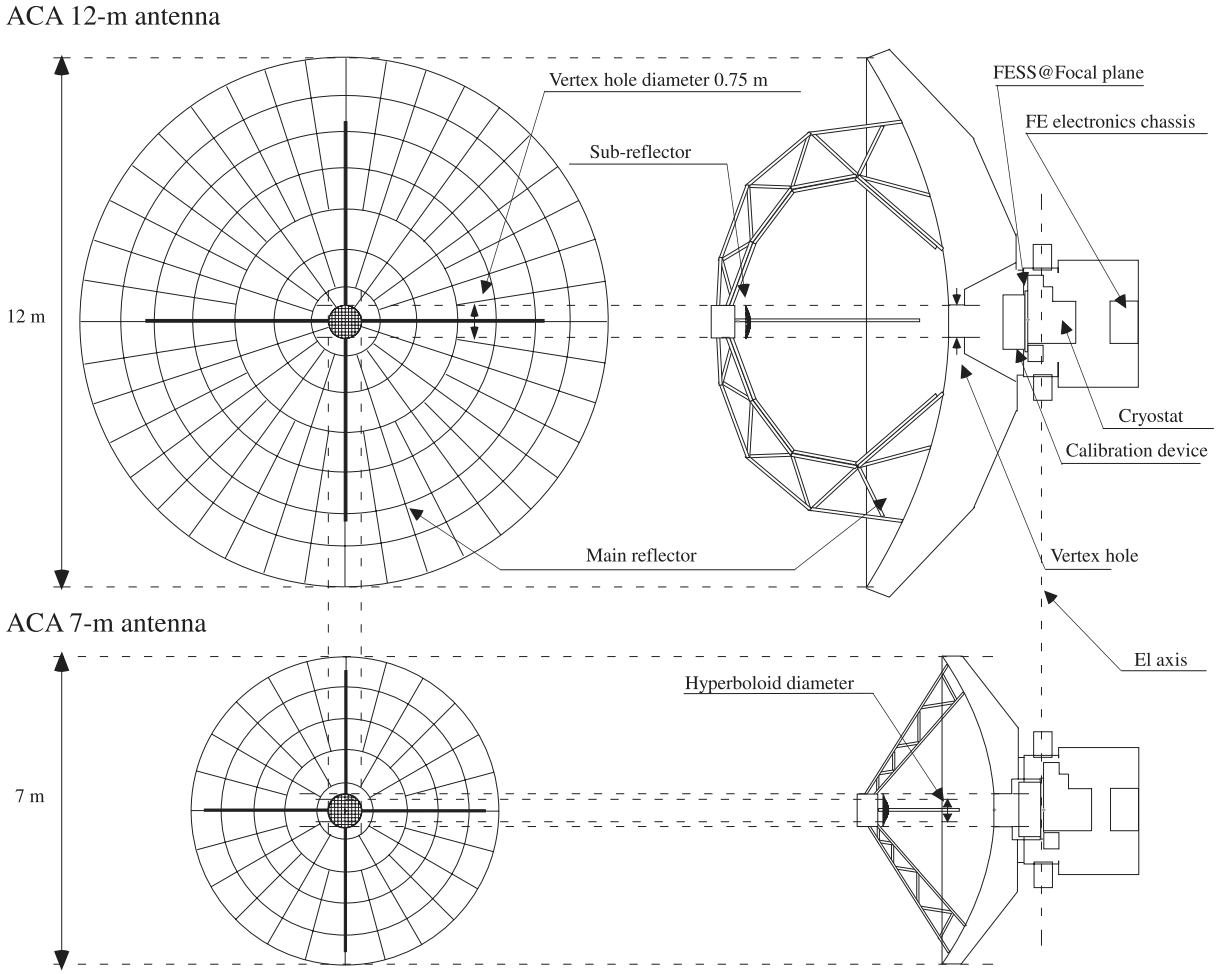

Fig. 6. Relations among the main reflector, the subreflector, and the antenna vertex hole (from table 3).

4.4.4. Ruze efficiency

Scattering due to surface inaccuracy accounts for the distortion of the wavefront. For a reflector with an rms deviation of the surface of $\varepsilon_{\rm fl}$, the Ruze efficiency at wavelength λ (see Ruze 1966) is

$$\eta_{\rm r} = \exp\left[-\left(\frac{4\pi\varepsilon_{\rm fl}}{\lambda}\right)^2\right]. \quad (8)$$

4.4.5. Blockage efficiency

Sub-subsection 4.3.1 shows that the 7 m antenna strongly comes under the influence of a vertex hole diameter of 0.75 m due to using the same FE subsystem as that of the 12 m antenna. Under such a condition, a decrease in blockage efficiency is essentially inevitable, mainly because the sensitive aperture center of the illumination is missing. The blockage efficiency is approximately derived from

$$\eta_{\rm b} = \frac{\int\int_{\rm a}|E_{\rm a}|^2 dS - \int\int_{\rm b}|E_{\rm b}|^2 dS}{\int\int_{\rm a}|E_{\rm a}|^2 dS}. \quad (9)$$

In the case of the condition described in sub-subsection 4.3.1, the blockage efficiencies of 12 m and 7 m antennas become 0.950 and 0.912, respectively.

4.4.6. Total aperture efficiency

The aperture efficiency is estimated from

$$\eta_{\rm a} = \eta_{\rm o}\eta_{\rm i}\eta_{\rm s}\eta_{\rm d}\eta_{\rm r}\eta_{\rm b}. \quad (10)$$

Table 4 lists several parameters to estimate the aperture efficiencies in frequency ranging from 31.3 GHz to 950 GHz for a comparison between 12 m antennas and 7 m antennas by using surface accuracies of 25 μm rms for the 12 m dishes and 20 μm rms for the 7 m dishes along with the illumination and spillover efficiencies that would result from a perfectly imaged, corrugated feed horn. The values of the illumination efficiency, spillover efficiency, and blockage efficiency (12 m antenna) are consistent with those from J. Lamb et al. (2001).[9]

Figure 7 shows the estimated aperture efficiency in the frequency range of 31.3 to 950 GHz if an ideal corrugated horn is perfectly imaged onto the subreflector. At 950 GHz, the 7 m antenna has a higher performance to achieve an aperture efficiency of 41.2%, rather than that of the 12 m antenna of 30.1% (see table 4). Although the 7 m antenna has a disadvantage of the geometrical blocking of 5% (see sub-subsection 4.3.1), these aperture efficiencies of the 12 m and 7 m antennas will be balanced at around 335 GHz. The aperture efficiency for the 7 m antenna becomes better than that of the 12 m antenna

Table 4.*

Frequency (GHz)	Radiation efficiency (%)	Illumination efficiency (%)	Spillover efficiency (%)	(12 m / 7 m) Diffraction efficiency (%)	(12 m / 7 m) Ruze efficiency (%)	(12 m / 7 m) Blockage efficiency (%)	(12 m / 7 m) Total aperture efficiency (%)
31.3	99.8	91.1	95.4	96.7 / 95.7	99.9 / 99.9	95.0 / 91.2	79.5 / 75.6
38	99.7	91.1	95.4	97.0 / 96.1	99.8 / 99.9	95.0 / 91.2	79.7 / 75.9
78	99.6	91.1	95.4	97.9 / 97.3	99.3 / 99.6	95.0 / 91.2	80.0 / 76.5
100	99.6	91.1	95.4	98.1 / 97.6	98.9 / 99.3	95.0 / 91.2	79.8 / 76.5
144	99.5	91.1	95.4	98.4 / 98.0	97.7 / 98.6	95.0 / 91.2	79.0 / 76.2
187	99.5	91.1	95.4	98.6 / 98.3	96.2 / 97.6	95.0 / 91.2	77.9 / 75.5
243	99.4	91.1	95.4	98.8 / 98.4	94.5 / 96.5	95.0 / 91.2	76.0 / 74.4
323	99.3	91.1	95.4	99.0 / 98.7	89.2 / 92.9	95.0 / 91.2	72.3 / 72.1
442	99.1	91.1	95.4	99.1 / 98.9	80.7 / 87.2	95.0 / 91.2	65.4 / 67.7
675	98.9	91.1	95.4	99.3 / 99.1	60.6 / 72.6	95.0 / 91.2	49.2 / 56.4
868	98.8	91.1	95.4	99.4 / 99.2	43.7 / 58.9	95.0 / 91.2	35.4 / 45.7
950	98.7	91.1	95.4	99.4 / 99.2	37.1 / 53.0	95.0 / 91.2	30.1 / 41.2

* Estimated aperture efficiencies for an ideal feed system with a corrugated horn in order to make a comparison between 12 m (25 μ rms) and 7 m (20 μ rms) antennas at the center frequency of radio frequency (RF) range of each cartridge, and the lowest and the highest frequencies of ALMA (see table 2).

at submillimeter wavelengths for Bands 7, 8, 9, and 10. After making estimations of the aperture efficiencies for all frequencies, the 12 m antenna will show aperture efficiencies of 79.5% at 31.3 GHz and 51.0% at 650 GHz, while the 7 m antenna will achieve aperture efficiencies of 75.6% at 31.3 GHz and 57.7% at 650 GHz. Taking several optics losses from the antenna to the receiver into consideration, we find that the 12 m antenna will have aperture efficiencies of better than 75% at 31.3 GHz and 45% at 650 GHz (Beasley et al. 2006), and that the 7 m antenna will have better aperture efficiencies than 70% at 31.3 GHz and 50% at 650 GHz.

Also, figure 8 shows the estimated effective apertures derived from figure 7.

4.5. Pointing Accuracy of Antennas

For the 12 m antenna, the primary beam at the "submillimeter workhorse" 345 GHz frequency (850 micron in wavelength) is about 18″, whereas at the highest frequency of 950 GHz it is only 6″. ACA is expected to play an important role in observing programs at high frequencies, where the field of view (F.O.V) is smaller than the astronomical objects, and thus the pointing error of the 12 m antenna will be very critical. Since the offset pointing error should be less than 1/10 of the full width at half maximum (FWHM) beam width, this specification of the 12 m antenna needs to be less than 0.″6 rms, compared with the beam width of 6″ (Beasley et al. 2006).

Simulations have shown that under the actual observing conditions, limited by antenna pointing errors, the maximum achievable fidelity for extended sources is significantly limited when using this method (e.g., Ekers 1999; J. Welch 2001[2]). Simulations so far clearly indicate that the addition of ACA into the 12 m Array improves the fidelity of the final images (T. Tsutsumi et al. 2004[10]; J. Pety et al. 2001a[11]; J. Pety et al. 2001b[12]) when all ACA antennas with pointing errors of 0.″6 rms are considered. Thus, the 7 m antenna also needs to be less than 0.″6 rms by taking into cosideration that an anomalous reflection of about 0.″5 at Chajnantor Altiplano is estimated.

4.6. Phase Stability

ACA has the capability of synthesis imaging up to 950 GHz. Three kinds of phase fluctuations need to be corrected to such a level, i.e., the atmosphere (mainly due to water-vapor fluctuations), the system for electronics (mainly due to LO), and the structure (mainly due to antenna). Phase calibration schemes using WVRs on each of TP Array antennas will be used for the atmosphere (see subsection 2.2), and moderate (about 100 s) switching to nearby calibrators will be used for the system.

The WVR-corrected visibility phase is expected to be accurate to 1 radian on 100 s time scales (expected length of synthesis cycles for the ACA only observations) at the highest frequency of 950 GHz, which corresponds to a delay path error of 50 μm rms. This requires the short-term delay path error, per antenna, due to the phase noise to be $< 0.707 \times 50 = 35\,\mu$m rms (is equal to a delay time error of 118 fs). Thus, the instrumental delay error, after all corrections, will be less than 22 μm (= 75 fs), which is less than the delay noise introduced by the atmosphere under the 95 percentile conditions ($< 0.707 \times 35 = 25\,\mu$m). By budgeting from the total instrumental error to the structure and the system for electronics, the nonrepeatable residual delay due to the structure for the antenna must be less than 15 μm rms when tracking an astronomical source at the sidereal rate (Beasley et al. 2006).

5. The Performance and Expected Science Enhancement of ACA

5.1. Sensitivity, Angular Resolution, and Field of View

The sensitivities at any observing frequencies at one

[10] ALMA memo No. 488 ⟨http://www.alma.nrao.edu/memos/html-memos/abstracts/abs488.html⟩.

[11] ALMA memo No. 387 ⟨http://www.alma.nrao.edu/memos/html-memos/abstracts/abs387.html⟩.

[12] ALMA memo No. 398 ⟨http://www.alma.nrao.edu/memos/html-memos/abstracts/abs398.html⟩.

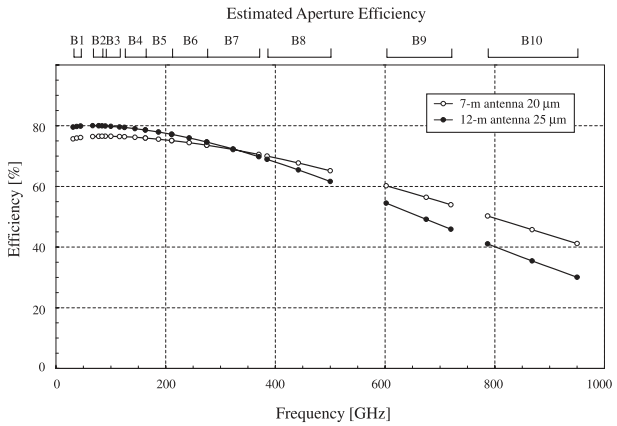

Fig. 7. Estimated total aperture efficiencies with 20 and 25 μm rms surface accurancies with the ALMA frequency coverage (see table 2) if an ideal corrugated horn is perfectly imaged onto the subreflector.

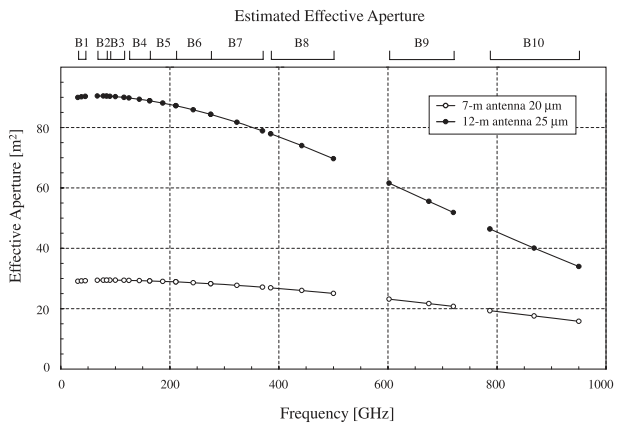

Fig. 8. Effective aperture areas of 7 m and 12 m antennas with the ALMA frequency coverage (see table 2) if an ideal corrugated horn is perfectly imaged onto the subreflector.

antenna are derived from the aperture efficiency (see subsubsection 4.4.6), the receiver efficiency ($\eta_{\rm rx}$) (referring to J. Lamb et al. 2001),[9] the system loss due to mainly the digitizing loss ($\eta_{\rm d}$) (Iguchi & Kawaguchi 2002 for quantization loss and requantization loss), the coherence loss ($\eta_{\rm c}$) after correcting with WVR (Rogers & Moran 1981 for calculation of the coherence loss, H. Kikuchi & S. Iguchi 2006[13] for derivation and estimation of Allan standard deviation from the ALMA phase-stability specification, as shown in subsection 4.6), the system noise temperature ($T_{\rm sys}$) (Iguchi 2005), including the antenna noise temperature under atmospheric condition at an altitude of 5050 m (e.g., figure 10), and the IF bandwidth (see subsection 4.2). By assuming natural weighting and antennas with the same diameter and system noise temperature, the rms thermal noise, $\Delta I_{\rm m}$, in the visibility amplitude of a single-polarization image can be derived as (referring to Thompson et al. 2001)

$$\Delta I_{\rm m} = \frac{\sqrt{2}k_{\rm B}T_{\rm sys}}{\eta A\sqrt{N(N-1)\Delta\nu\Delta t}}, \tag{11}$$

where A is the antenna aperture of one element antenna [m^2], N is the number of ACA antennas available for use, $k_{\rm B}$ is the Boltzmann constant, $T_{\rm sys}$ is the system noise temperature at the 2SB receiving system [K], η is the product of $\eta_{\rm a}\eta_{\rm rx}\eta_{\rm d}\eta_{\rm c}$, $\Delta\nu$ is the bandwidth [Hz], and Δt is the total integration time on source [s]. In the case of the ACA full Array, the equation can be represented by

$$\Delta I_{\rm m} = \frac{k_{\rm B}T_{\rm sys}}{\sqrt{A_{\rm full}\Delta\nu\Delta t}}, \tag{12}$$

$$A_{\rm full} = 66(\eta_7 A_7)^2 + 6(\eta_{12}A_{12})^2 + 48(\eta_7\eta_{12}A_7A_{12}), \tag{13}$$

where 66 is the number of baselines of the 7 m Array, 6 is the number of baselines of the TP Array, and 48 is the number of baselines between the 12 m and 7 m antennas.

Plots of the uv plane coverage and the synthesized beam patterns with the 7 m Array and the ACA full Array for sources at an hour angle range of -3 to $+3$ hr and declinations of $-78°$, $-53°$, $-23°$, $7°$, and $32°$ are shown in figure 9. Figure 9a shows a dotted-line circle equivalent to the baseline length of 6 m, which is half of the diameter of the 12 m antenna for the TP Array. This indicates an area mainly covered by the 12 m antenna of the TP Array as a single-dish mode, and shows that ACA under the coordinated operation mode can continuously cover the baselines of zero to about 33 m (such as figure 3).

An image made from the uv plane track will have a synthesized beam with a slightly narrower minor axis of FWHM, which is written by

$$\theta_{\rm res} = h_{uv}\frac{\lambda}{B_{\rm m}}, \tag{14}$$

where λ is the observing wavelength [mm], $B_{\rm m}$ is a maximum baseline length in array [mm], and h_{uv} is a factor determined by the distribution of plots on the uv plane. The factor can be estimated with the synthesized beam patterns calculated from the uv plot data. From figure 9, the parameters of the synthesized beam are listed in table 5. It was confirmed that there are no large discrepancies between our results and those at an h_{uv} of 0.7 (derived in Thompson et al. 2001). By taking these estimated results into consideration, the angular resolution of ACA can be represented as follows:

$$\theta_{\rm res} \sim 5\frac{\lambda\ [\rm mm]}{1\ [\rm mm]}\quad [\rm arcsec]\quad \text{for 7 m Array}, \tag{15}$$

$$\sim 3\frac{\lambda\ [\rm mm]}{1\ [\rm mm]}\quad [\rm arcsec]\quad \text{for ACA full Array}. \tag{16}$$

The ultimate factor limiting the field-of-view ($\theta_{\rm fov}$) is the diffraction-limited response of the individual antennas (Thompson et al. 2001). This means that the field-of-view of an interferometer corresponds to the beam FWHM of an antenna with a diameter of D [mm] ($\theta_{\rm beam}$). Thus, the field-of-view of an interferometer is written as

$$\theta_{\rm fov} = \theta_{\rm beam} = 1.2\frac{\lambda}{D}, \tag{17}$$

where the factor of 1.2 is suitable for an edge taper of 12 dB (Goldsmith 1998).

The imaging sensitivity, field of view, and synthesized beam

[13] ALMA memo No. 545 ⟨http://www.alma.nrao.edu/memos/html-memos/abstracts/abs545.html⟩.

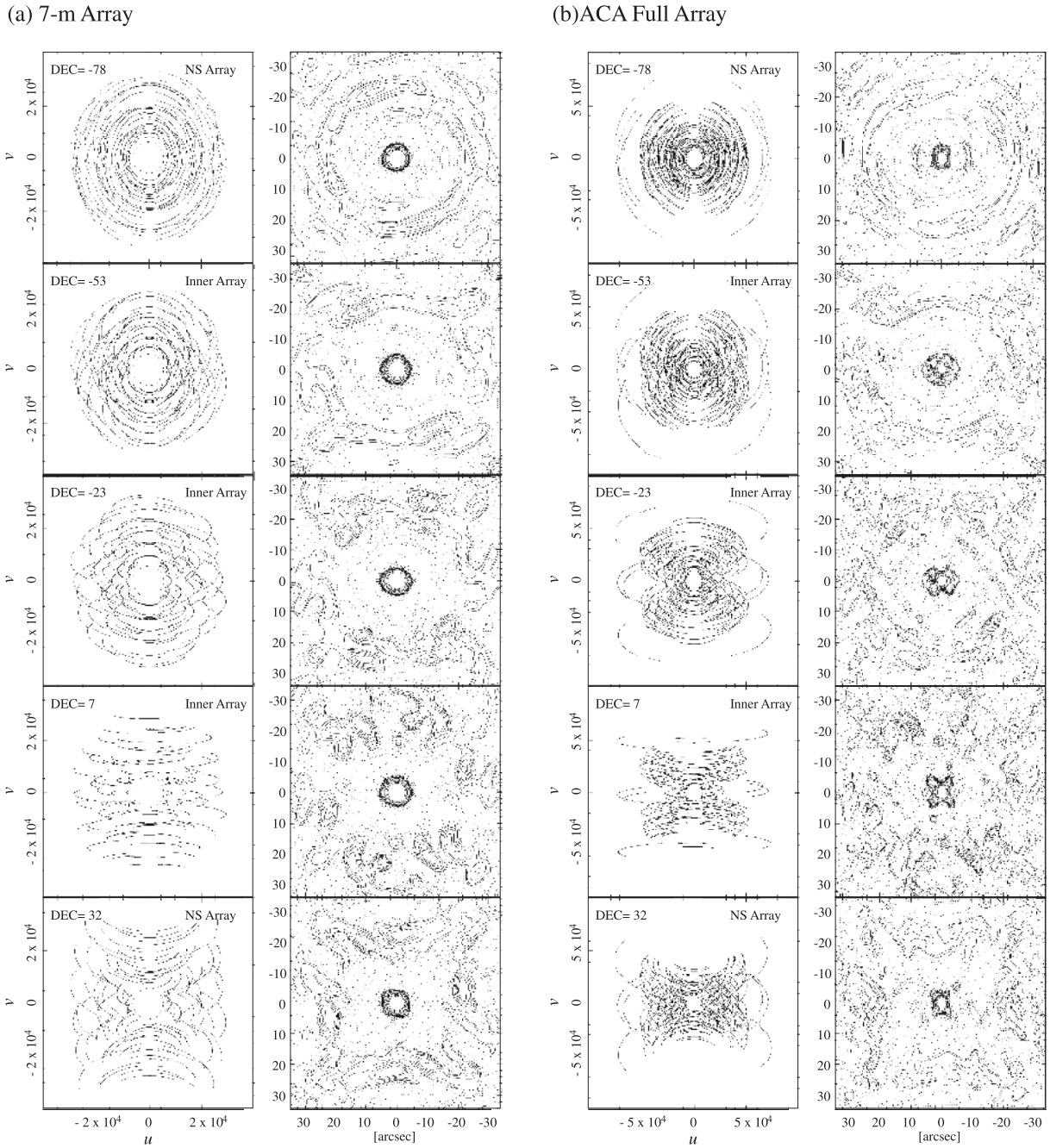

Fig. 9. The *uv* plane coverages and their synthesized beam patterns at (a) the 7 m Array and (b) the ACA full Array with the observing wavelength of 1 mm, hour angle range of −3 to +3 hr, and five declinations of −78°, −53°, −23°, 7°, and 32° with NS, Inner, Inner, Inner, and NS Arrays, respectively. In simulating each *uv* plane coverage, plots at the integration period of 60 s are flagged by an elevation limit of 2° and shadowing at a compact configuration. Each *uv* plane coverage for the 7 m Array (a) shows a dotted-line circle equivalent to the baseline length of 6 m in comparison with the *uv* response of 12 m antenna in the TP Array. The contour levels in each synthesized beam pattern are −20, −15, −10, −8, −6, −4, −2, −1, 1, 2, 4, 6, 8, 10, 15, 20, 30, 40, and 50 percents.

for the stand-alone mode are presented in table 6. The sensitivities of Band 9 and Band 10 are less than those of the other Bands, because the opacities are too large compared with the others (see figure 10), and also the coherence losses are larger. Although there are many absorption lines, the high sensitivity in Band 8 will be realized by avoiding them and carefully selecting the observing frequency.

5.2. *ALMA Scientific Enhancements by ACA*

ALMA will image cold molecular gas and dust in the Universe, from which stars, planets, and galaxies are formed. In addition, ALMA will also be able to image atomic gas where molecular clouds are thought to be formed. The emission from such gases and dust are mostly thermal (except for special cases, such as molecular maser emission). For most

Table 5.*

Inner or NS array	Declination (°)	7 m Array Major axis (″)	7 m Array Minor axis (″)	7 m Array PA (°)	ACA full Array Major axis (″)	ACA full Array Minor axis (″)	ACA full Array PA (°)
NS Array	−78°	4.75	4.54	115.°0	3.95	2.93	0.°9
Inner Array	−53°	5.15	4.92	89.°8	4.17	3.54	4.°2
Inner Array	−23°	5.17	4.38	90.°3	3.71	3.60	90.°1
Inner Array	7°	5.24	5.00	246.°9	4.02	3.58	13.°2
NS Array	32°	4.73	4.53	64.°2	4.02	2.85	7.°5

* The synthesized beams for the 7 m Array and the ACA full Array at the observing wavelength of 1 mm (derived from figure 9).

Table 6.*

Band	Frequency (GHz)	7 m Array $\Delta I_{\rm m}$ (mJy beam^{-1})	7 m Array $\theta_{\rm fov}$ (″)	7 m Array $\theta_{\rm res}$ (″)	ACA full Array $\Delta I_{\rm m}$ (mJy beam^{-1})	ACA full Array $\theta_{\rm fov}$ (″)	ACA full Array $\theta_{\rm res}$ (″)
Band 3	94	3.1	113	16	1.6	66	9.6
Band 4	145	4.3	73	10	2.1	43	6.2
Band 6	224	6.7	47	6.7	3.3	28	4.0
Band 7	345	16	31	4.3	8.1	18	2.6
Band 8	410	27	26	3.7	14	15	2.2
Band 9	670	190	16	2.2	102	9	1.3
Band 10	860	365	12	1.7	206	7	1.0

* Field of view ($\theta_{\rm fov}$), angular resolution ($\theta_{\rm res}$), and single point-source sensitivity ($\Delta I_{\rm m}$) for continuum observations with ACA. The 1 second on-source integration, 8 GHz bandwidth at a single polarization, and 25-percentile atmosphere at main atmospheric windows (see figure 10) are assumed.

of these objects, spatially resolved observations are desirable, and collecting the extended emission is critical to quantitative studies, such as estimating the gas mass or column density profile using thermal emission. The high fidelity of imaging of ALMA will be complemented with information provided by ACA at short spacings. For instance, ACA is expected to fulfill the aim and to play an important scientific role in the observation of low-mass star-formation ranging from prestellar cores and protostellar envelopes to debris disks (Takakuwa et al. 2008).

ALMA will be able to measure magnetic fields (morphology and strengths) in molecular cloud cores or envelopes through polarization mapping (i.e., measurements of Stokes parameters), in which stars and protoplanetary disks have been formed. Since polarized emission from dust is usually as small as a few to 10 percents of the total flux, the measurements require both high sensitivity and high accuracy. ALMA has so great potential as to draw polarization mapping and to answer interesting long-standing questions about the roles of magnetic fields in the interstellar medium (e.g., the angular-momentum problem in star formation and the origin and mechanism of bipolar outflows). The missing total and polarized fluxes at short and zero baselines will also pose a similar problem to that in the case discussed in the previous section 2. Simulations of imaging performance in polarization show that the inclusion of ACA can significantly improve the fidelity.

6. Summary

ACA is being built to enhance the science of the ALMA 12 m Array only by significantly improving the image fidelity. ACA consists of four 12 m-diameter antennas for total power observations (TP Array) and twelve 7 m-diameter antennas for an interferometer (7 m Array). The antennas are all movable using a specially designed antenna transporter among 22 prepared antenna stations. The TP Array is capable of taking single-dish images that contain information about the zero-meter baseline. The 7 m Array antenna configuration is arranged to make up for a uv gap of 6 to 15 m between the 12 m Array and the TP Array. Thus, ALMA with ACA will be able to achieve high fidelity of imaging, particularly for extended astronomical sources.

There are three types of ACA observation modes: the coordinated operation as a major observing mode of ALMA, the combined operation for improving the point-source sensitivity and the achievement of high-quality ACA calibration accuracy, and the ACA stand-alone operation. According to scientific justifications, the ACA observation modes can be selected and then operated.

The system requirements are compatible between the 12 m Array and ACA according to the ALMA operation concepts and scientific requirements: e.g., interface, frequency coverage, receiving system, IF system, correlation, pipeline and reduction software, etc. Two types of antennas with

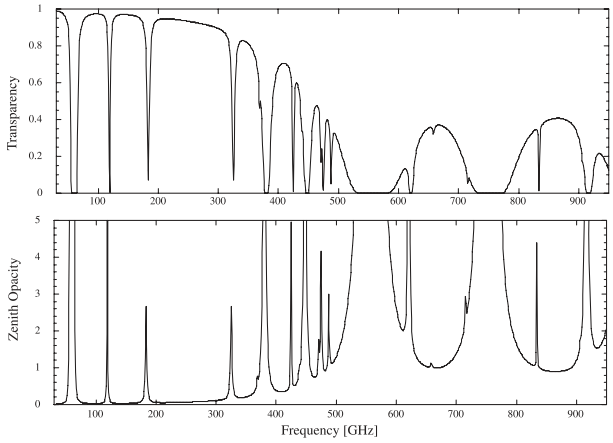

Fig. 10. Atmospheric transparency (top) and the zenith atmospheric opacity (bottom) at the ALMA site with the water vapor content of 1 mm, which were modeled by Pardo, Cernicharo, and Serabyn (2001).

different diameters of 12 m and 7 m are developed. The 12 m antenna will have aperture efficiencies of 75% at 31.3 GHz and 45% at 650 GHz at surfaces with an rms deviation from the ideal of 25 μm rms or less, while the 7 m antenna will achieve aperture efficiencies of 70% at 31.3 GHz and 50% at 650 GHz by meeting the surfaces with an rms deviation from the ideal of 20 μm rms or less. Each antenna is fully steerable and designed for an offset-pointing accuracy of less than $0\farcs6$ and a path-length error of less than 15 μm during sidereal tracking. Some comparisons of parameters between the 12 m antenna and 7 m antenna, related to the main specifications, are summarized in table 7.

Table 7. The main specifications of the ALMA antenna.

Specs	12 m antenna	7 m antenna
Diameter	12 m	7 m
Vertex hole size	0.75 m	
F/D	0.4	0.37
Geometrical blockage	$<3\%$	$<5\%$
Surface accuracy	$<25\,\mu$m rms	$<20\,\mu$m rms
Aperture efficiency at 675 GHz	>0.45	>0.50
Offset pointing	$<0\farcs6$ rms	
Path length error	$<15\,\mu$m during sidereal track	
Close packing ratio	1.25	

The authors would like to acknowledge ALMA colleagues for helpful technical discussions. The authors would like to express their gratitude to James M. Moran who provided constructive comments and suggestions concerning this paper.

References

Beasley, A. J., Murowinski, R., & Tarenghi, M. 2006, Proc. SPIE, 6267, 626702
Cornwell, T. J. 1988, A&A, 202, 316
Ekers, R. D. 1999, ASP Conf. Ser., 180, 321
Escoffier, R. P., et al. 2007, A&A, 462, 801
Goldsmith, P. F. 1998, Quasioptical Systems: Gaussian Beam Quasioptical Propagation and Applications (New York: IEEE Press)
Iguchi, S. 2005, PASJ, 57, 643
Iguchi, S., & Kawaguchi, N. 2002, IEICE Trans. Commun., E85-B, 1806
Kildal, P.-S. 1983, IEEE Trans. Antennas Propag., 31, 903
Morita, K.-I., & Holdaway, M. A. 2008, Proc. SPIE, 7012, 70120O
Pardo, J. R., Cernicharo, J., & Serabyn, E. 2001, IEEE Trans. Antennas Propag., 49, 1683
Rogers, A. E. E., & Moran, J. M., Jr. 1981, IEEE Trans. Instrum. Meas., 30, 283
Ruze, J. 1966, Proc. IEEE, 54, 633
Takakuwa, S., Iono, D., Vila-Vilaro, B., Sekiguchi, T., & Kawabe, R. 2008, Ap&SS, 313, 169
Thompson, A. R., Moran, J. M., & Swenson, G. W., Jr. 2001, Interferometry and Synthesis in Radio Astronomy, 2nd ed. (New York: John Wiley & Sons)
Vanden Bout, P. A. 2005, in Proc. of the Dusty and Molecular Universe, ed. A. Willson (Noordwijk: ESA Publications Division), 23